Received: 28 August 2024 | Revised: 11 October 2024 | Accepted: 15 October 2024

DOI: 10.1002/nbm.5284

RESEARCH ARTICLE

NMR IN BIOMEDICINE WILEY

Simultaneous assessment of cerebral glucose and oxygen metabolism and perfusion in rats using interleaved deuterium (^{2}H) and oxygen-17 (^{17}O) MRS

Guangle Zhang | Parker Jenkins | Wei Zhu | Wei Chen | Xiao-Hong Zhu

Center for Magnetic Resonance Research (CMRR), Department of Radiology, University of Minnesota, Minneapolis, Minnesota, USA

Correspondence
Xiao-Hong Zhu, Center for Magnetic Resonance Research (CMRR), Department of Radiology, University of Minnesota, 2021 6th St SE, Minneapolis, MN 55455, USA.
Email: zhuxx022@umn.edu

Funding information
National Institutes of Health (NIH), Grant/Award Numbers: R01 MH111413, R01 NS133006, R01 CA240953, S10 RR025031, P41 EB027061

Abstract

Cerebral glucose and oxygen metabolism and blood perfusion play key roles in neuroenergetics and oxidative phosphorylation to produce adenosine triphosphate (ATP) energy molecules in supporting cellular activity and brain function. Their impairments have been linked to numerous brain disorders. This study aimed to develop an in vivo magnetic resonance spectroscopy (MRS) method capable of simultaneously assessing and quantifying the major cerebral metabolic rates of glucose (CMR_{Glc}) and oxygen ($CMRO_2$) consumption, lactate formation (CMR_{Lac}), and tricarboxylic acid (TCA) cycle (V_{TCA}); cerebral blood flow (CBF); and oxygen extraction fraction (OEF) via a single dynamic MRS measurement using an interleaved deuterium (^{2}H) and oxygen-17 (^{17}O) MRS approach. We introduced a single-loop multifrequency radio-frequency (RF) surface coil that can be used to acquire proton (^{1}H) magnetic resonance imaging (MRI) or interleaved low-γ X-nuclei ^{2}H and ^{17}O MRS. By combining this RF coil with a modified MRS pulse sequence, ^{17}O-isotope-labeled oxygen gas inhalation, and intravenous ^{2}H-isotope-labeled glucose administration, we demonstrate for the first time the feasibility of simultaneously and quantitatively measuring six important physiological parameters, CMR_{Glc}, $CMRO_2$, CMR_{Lac}, V_{TCA}, CBF, and OEF, in rat brains at 16.4 T. The interleaved ^{2}H–^{17}O MRS technique should be readily adapted to image and study cerebral energy metabolism and perfusion in healthy and diseased brains.

KEYWORDS
brain energy metabolism and perfusion, interleaved ^{2}H–^{17}O MRS technique, multifrequency RF surface coil, ultrahigh field, X-nuclear MRS and imaging

1 | INTRODUCTION

The brain is one of the most metabolically active organs in the body, using glucose as its primary energy source.[1] It accounts for only 2% of an adult's body weight (BW) but consumes approximately 20% of the body's total glucose and oxygen consumption at rest.[2] Glucose is delivered to the brain through circulating blood and crosses the blood–brain barrier via glucose transporters. Once inside the brain cells, glucose is metabolized through the

Abbreviations: ^{13}C, carbon-13; ^{17}O, oxygen-17; ^{1}H, proton; ^{2}H, deuterium; ^{31}P, phosphorus-31; CBF, cerebral blood flow; CMR_{Glc}, cerebral metabolic rate of glucose consumption; CMR_{Lac}, cerebral metabolic rate of lactate formation; $CMRO_2$, cerebral metabolic rate of oxygen consumption; CSI, chemical shift imaging; GEMS, gradient-echo multiple slice; HDO, deuterated water; OEF, oxygen extraction fraction; RF, radio frequency; SNR, signal-to-noise ratio; SPULS, single-pulse acquire sequence; TCA, tricarboxylic acid; V_{TCA}, cerebral metabolic rate of the TCA cycle.

glycolytic pathway to form two pyruvate molecules, which are an important intermediate in glucose metabolism, and this metabolic activity can be quantified by the cerebral metabolic rate of glucose consumption (CMR_{Glc}). Pyruvate can be converted into lactate via lactate dehydrogenase in the cytoplasm, a reaction that can occur in the presence of oxygen in a healthy brain and is therefore termed aerobic glycolysis. This conversion, measurable by the cerebral metabolic rate of lactate formation (CMR_{Lac}), generates only two energy molecules of adenosine triphosphate (ATP) per consumed glucose. Normally, the majority of pyruvate can be converted to acetyl-CoA by pyruvate dehydrogenase and then enter the tricarboxylic acid (TCA) cycle occurring inside mitochondria, a biochemical process that can be quantified by the cerebral metabolic rate of the TCA cycle (V_{TCA}). The TCA cycle supports oxidative phosphorylation, which is closely related to oxygen usage (measurable by the cerebral metabolic rate of oxygen consumption [$CMRO_2$]), and produces over 30 ATP molecules per consumed glucose.[3,4] Figure 1A summarizes the main metabolic pathways and associated rates of brain glucose energy metabolism, including non-oxidative (CMR_{Glc} and CMR_{Lac}) and oxidative (V_{TCA} and $CMRO_2$) metabolic processes and perfusion process (measurable by the cerebral blood flow [CBF]). There is an unmet need to develop a noninvasive method that enables quantitative assessment of these major metabolic rates, CBF, and oxygen extraction fraction (OEF) ideally from a single in vivo measurement.

In vivo X-nuclear (e.g., phosphorus-31 (^{31}P), carbon-13 (^{13}C), deuterium (^{2}H), and oxygen-17 (^{17}O)) magnetic resonance spectroscopy (MRS) or imaging techniques are promising for studying cerebral metabolism and bioenergetics in animal and human brains.[2,5–9] Their detection sensitivities and capabilities are significantly improved at high/ultrahigh fields.[10–12] However, these technologies are often used separately to gather limited information from the resonance signals of metabolites associated with the desired nucleus. Performing interleaved or simultaneous multi-nuclei measurements is challenging, hindering the ability to capture comprehensive metabolic and hemodynamic information in the same brain and MRS scan session.

One essential component of X-nuclear MRS measurement is the dual-frequency radio-frequency (RF) coil, which can be operated at the proton (^{1}H) Larmor frequency for acquiring brain anatomic images and performing magnetic field (B_0) shimming and at an X-nuclear Larmor frequency for acquiring MRS. Including multiple RF surface coils[13] tuned to the desired multiple resonant frequencies in an RF coil probe creates technical challenges because it is difficult to decouple them electronically. This complexity in the coil structure may degrade coil performance or require manual tuning of a single coil to multiple frequencies at a given time,[2,13–19] thus challenging to achieve rapid frequency switching between different MRS operation frequencies, making it difficult to capture time-sensitive multi-nuclei metabolic information and dynamics through interleaved or simultaneous scans.

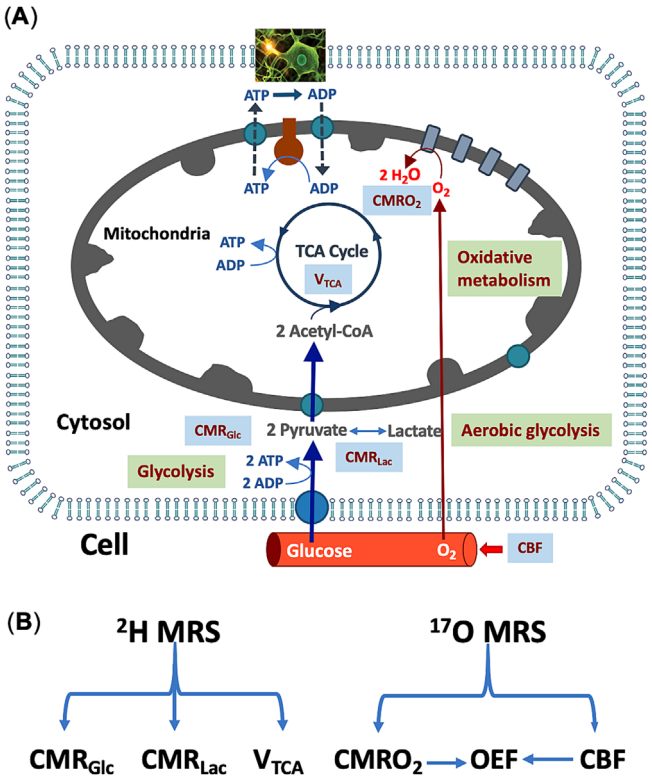

FIGURE 1 Quantitative assessment of cerebral perfusion, cerebral energy metabolism, and metabolic rates along key metabolic pathways using an interleaved ^{2}H–^{17}O magnetic resonance spectroscopy (MRS) approach. (A) Glucose is supplied and transported via the circulating blood flow to brain cells, where it is metabolized via cytosolic glycolysis and the mitochondrial tricarboxylic acid (TCA) cycle, coupled with oxygen metabolism and oxidative phosphorylation to generate adenosine triphosphate (ATP) molecules in supporting neuronal activity and brain function. (B) Dynamic changes in ^{2}H-labeled metabolite signals measured by in vivo ^{2}H MRS enable the estimation of the three cerebral metabolic rates of glucose consumption (CMR_{Glc}), lactate formation (CMR_{Lac}), and TCA cycle activity (V_{TCA}). In parallel, dynamic changes in the ^{17}O-labeled metabolic water signal facilitate the estimation of the cerebral metabolic rate of oxygen consumption ($CMRO_2$), cerebral blood flow (CBF), and oxygen extraction fraction (OEF $\propto$ $CMRO_2$/CBF). ADP, adenosine diphosphate.

In this study, we developed a single-loop RF surface coil with active tuning/matching capability to facilitate ^{1}H magnetic resonance imaging (MRI) and interleaved ^{2}H–^{17}O MRS measurements of rat brains at 16.4 T. By integrating dynamic ^{2}H–^{17}O MRS acquisitions with ^{2}H-labeled glucose administration and ^{17}O-labeled oxygen gas inhalation, we demonstrated for the first time the feasibility of simultaneously measuring and quantifying six key neurophysiological parameters: CMR_{Glc}, CMR_{Lac}, and V_{TCA} from dynamic ^{2}H MRS data and $CMRO_2$, CBF, and OEF from dynamic ^{17}O MRS data, both obtained from the same in vivo measurement, as illustrated in Figure 1B.

2 | METHODS

Firstly, we designed and constructed a prototype single-loop multifrequency surface coil that can operate at the ^{1}H Larmor frequency for acquiring brain anatomic images and performing B_0 shimming and also allow rapid switch between ^{2}H and ^{17}O Larmor frequencies via a circuit controller.[20,21] The coil performance was first tested on bench, and then a phantom test was conducted to validate the functionality of both the hardware (i.e., MRI scanner, RF coil, and circuit controller) and software (i.e., MRS pulse sequences) essential for the in vivo study using the rat brain model. Lastly, two sets of in vivo rat brain experiments were conducted by placing the RF coil on top of the animals' heads for the proof of concept of the interleaved ^{2}H–^{17}O MRS technique. The first in vivo experiment involved intravenous infusion of isotope-enriched D_2O and $H_2{}^{17}O$ water as dual-perfusion tracers[22] to evaluate the sensitivity, quality, and reliability of the acquired ^{2}H and ^{17}O MRS data. The second set of in vivo experiments used intravenous administration of deuterium-labeled D-glucose-6,6-d_2 (D66) in parallel with an inhalation of ^{17}O-labeled $^{17}O_2$ gas to explore the feasibility of simultaneously assessing cerebral glucose and oxygen metabolic rates, CBF, and OEF in the rat brain. All MRI/MRS experiments were conducted using a 16.4-T/26-cm-bore-size animal MRI scanner (Varian/VNMRJ, California) equipped with a newly designed and constructed multifrequency RF surface coil. All animal studies were conducted in strict accordance with the Guide of the National Research Council for the Care and Use of Laboratory Animals. The Institutional Animal Care and Use Committee of the University of Minnesota approved the protocol.

2.1 | Coil design and bench test

To obtain a wide frequency tuning capability, a conventional single-loop RF coil loop of approximately 2.5 cm in diameter was connected to a tuning-matching circuit via two short copper wires with the desired length, used as an isolating inductor (L_1) to form two primary resonant circuits: One resonates at a very high ^{1}H Larmor frequency (698 MHz at 16.4 T), and the other resonates at a lower frequency range covering the ^{17}O (94 MHz) and ^{2}H (107 MHz) Larmor frequencies, as shown in Figure 2A,B (details about the coil design can be found in the literature[20,23]). To enable interleaved ^{2}H–^{17}O MRS measurements, a positive-intrinsic-negative (PIN)-diode circuit (controller) was added to actively switch the coil

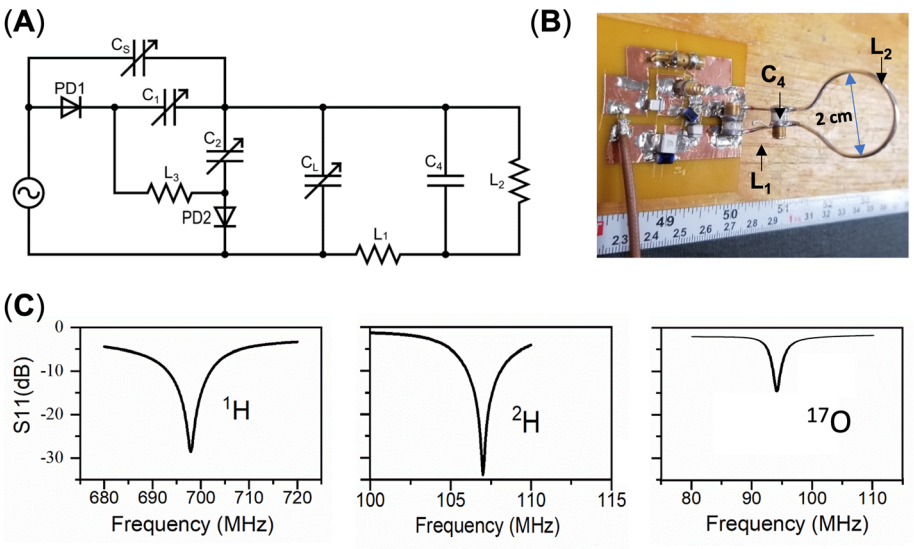

FIGURE 2 (A) Schematic circuit diagram of the multifrequency coil design. For ^{1}H (with positive-intrinsic-negative [PIN] diodes off), adjust C_S and C_L to tune and match the coil resonant frequency to 698 MHz at 16.4 T; for ^{2}H (with PIN diodes off), tune and match C_S and C_L to the ^{2}H operation frequency at 107 MHz; and for ^{17}O, ensure that the setup for ^{2}H is established, then apply a direct current (DC) and activate the PIN diodes, and use additional C_1 and C_2 to tune and match to the ^{17}O operation frequency at 94 MHz. (B) Photo of the prototype coil. (C) S11 parameters measured using the network analyzer with the coil tuned to the three targeted resonant frequencies: 698 MHz (^{1}H), 107 MHz (^{2}H), and 94 MHz (^{17}O).

operation frequency between the ^{2}H and ^{17}O resonant frequencies.[21] By introducing additional direct current (DC) input combined with the RF power provided by the coaxial cable, biasing the diode became feasible. This design allows for the RF current to flow through two capacitors (C_1, C_2), thereby increasing the capacitance of the tuning capacitors (C_L plus C_2) and the matching capacitors (C_S plus C_1), enabling dropping the coil resonant frequency from 107 MHz (^{2}H) to 94 MHz (^{17}O), creating an active tuning/matching mechanism that rapidly switches (<100 μs) the RF coil operation mode between ^{2}H and ^{17}O resonant frequencies (Figure 2A). In this study, the ^{1}H and ^{2}H resonant frequencies were initially tuned and matched manually under the loaded condition, whereas automatic tuning and matching of the ^{17}O resonant frequency was achieved through an actively tuning/matching PIN-diode circuit (Figure 2A). Using the single-loop multifrequency RF coil design and the circuit controller, the coil can work for $^{1}H/^{2}H/^{17}O$ triple resonant frequencies. The performance of the RF coil circuit was simulated using Keysight's ADS RF software, employing carefully selected electronic component values designed to minimize reflection coefficients at the triple targeted resonant frequencies. Subsequently, the RF coil circuit was built to specifications with traps added to reduce coaxial cable interference. The $^{1}H/^{2}H/^{17}O$ multifrequency surface coil was validated on bench using a network analyzer by measuring the reflection coefficients.

2.2 | Phantom test

The $^{1}H/^{2}H/^{17}O$ multifrequency surface coil underwent MRS testing at 16.4 T using a spherical phantom (2-cm diameter) filled with deionized water. ^{1}H MRI was performed using a multi-slice two-dimensional (2D) gradient-echo multiple slice (GEMS) imaging sequence with the following acquisition parameters: repetition time (TR)/echo time (TE) = 100 ms/4 ms, nominal RF pulse flip angle (FA) = 20°, field of view (FOV) = 30 mm × 30 mm, slice thickness = 1 mm, and matrix = 128 × 128. RF pulse power calibration and B_0 shimming were performed before the ^{1}H MRI and ^{2}H–^{17}O MRS acquisitions.

We conducted interleaved ^{2}H–^{17}O MRS measurements using a modified single-pulse acquire sequence (SPULS; Figure 3A), with each data block repeated 20 times for signal averaging. Each repetition consists of six segments (each lasting 50 ms): Five ^{17}O free-induction-decay (FID) acquisitions were captured when the RF coil and RF pulse carry frequency were switched to the ^{17}O Larmor frequency when the PIN didoes were short, and then one ^{2}H FID was collected when the RF coil and RF pulse carry frequency were switched back to the ^{2}H Larmor frequency when the PIN didoes were open. The apparent TRs were 300 ms for ^{2}H and 50 ms for ^{17}O. Key MRS acquisition parameters include a spectral width (SW) of 4006 Hz, an FID acquisition time (AT) of 44 ms, an RF hard pulse width of 200 μs, and an average (nt) of 20 FIDs for ^{2}H and 100 FIDs for ^{17}O across 20 repetitions (Figure 3A). The longitudinal relaxation time (T_1) of deuterium water (HDO) in the rat brain at 16.4 T is approximately 360 ms,[6] whereas the T_1 of $H_2{}^{17}O$ is less than 10 ms.[2] Therefore, the RF pulse FA was optimized to a 64° Ernst angle for acquisition of ^{2}H FIDs under partially saturated conditions and a nominal 90° FA for acquisition of ^{17}O FIDs under fully relaxed conditions.

To evaluate the performance of the interleaved ^{2}H–^{17}O MRS measurements, we collected control ^{2}H and ^{17}O MRS data from the phantom separately using the original SPULS sequence and the same acquisition parameters used in the interleaved ^{2}H–^{17}O MRS measurements. All obtained FIDs, whether using original or modified SPULS sequences, underwent the same signal processing. Additionally, interleaved ^{2}H–^{17}O MRS scans were averaged to ensure the same signal average as the control ^{2}H or ^{17}O MRS acquisition for performance comparison.

2.3 | Rat brain experiment with bolus administration of D_2O and $H_2{}^{17}O$ as perfusion tracers

A Sprague Dawley rat was anesthetized with 2% isoflurane in a mixture of N_2O/O_2 (about 3:1 volume ratio) and mechanically ventilated to maintain stable physiology during MRI/MRS measurements. The rat received 0.5 mL of deuterium-labeled water (D_2O, 99.8% enrichment) mixed with 3 mL of ^{17}O-isotope-labeled water ($H_2{}^{17}O$, approximately 2% enrichment) via femoral vein infusion. The interleaved ^{2}H–^{17}O MRS pulse sequence (Figure 3A) was used to acquire dynamic ^{2}H and ^{17}O MRS FIDs with the following acquisition parameters: for ^{2}H, TR = 300 ms, nt = 1, SW = 4006 Hz, AT = 44 ms, and FA = 64° (Ernst angle); for ^{17}O, TR = 50 ms, nt = 5, SW = 4006 Hz, AT = 44 ms, and FA = 90°. Dynamic ^{2}H–^{17}O MRS data acquisition lasted 30 min and included a 1-min baseline, 6-min dual-perfusion tracer infusion, and a 23-min post-infusion period. Prior to Fourier transformation, all ^{2}H and ^{17}O FIDs were subjected to 15-Hz line broadening to enhance the spectral signal-to-noise ratio (SNR). The decay rate constants (k) of the HDO and $H_2{}^{17}O$ water resonance intensities measured from the post-infusion spectra were determined by fitting the water resonance signals to an exponential function. These k values were utilized to approximately represent the apparent CBF values.

2.4 | Rat brain experiments with D66 administration and $^{17}O_2$ inhalation for studying cerebral glucose metabolism and perfusion

Two Sprague Dawley rats were mechanically ventilated under 2% isoflurane anesthesia in a mixture of N_2O/O_2 to maintain physiological conditions during MRI/MRS measurements. D66 (Cambridge Isotope Lab; 99% enrichment, 1 g/kg dissolved in 1.8 mL saline) was intravenously

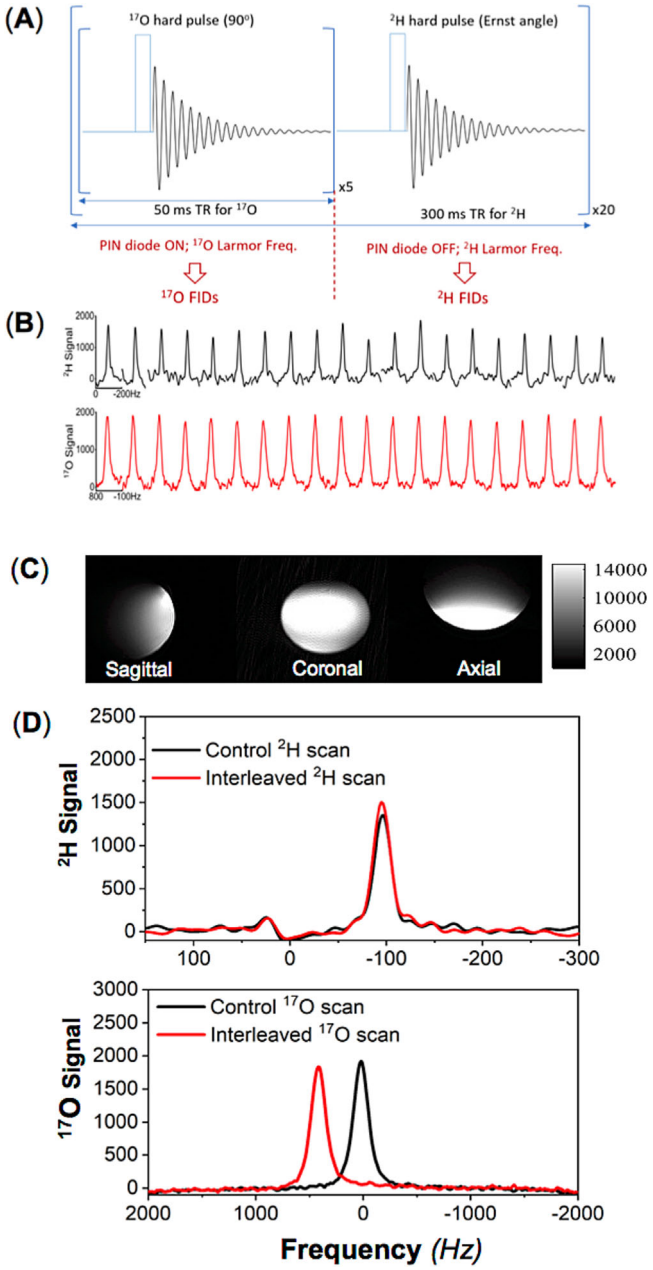

FIGURE 3 (A) Schematic representations of the modified single-pulse acquire sequence and parameter configurations for the interleaved ^{17}O–^{2}H magnetic resonance spectroscopy (MRS) acquisitions using the novel radio-frequency (RF) coil (Figure 2A,B), which can be operated at $^{17}O/^{2}H/^{1}H$ multifrequencies. (B) Sequential ^{2}H (nt = 1 × 20, top) and ^{17}O (nt = 5 × 20, bottom) spectra obtained from a natural abundance water phantom scanned using the interleaved ^{17}O–^{2}H MRS technique. Phantom test results of (C) ^{1}H magnetic resonance imaging (MRI) acquired with a two-dimensional (2D) gradient-echo multiple slice (GEMS) imaging sequence and (D) averaged ^{2}H (top panel, nt = 20) and ^{17}O (bottom panel, nt = 100) signals from control scans (in black) and interleaved ^{2}H–^{17}O scans (in red) of natural abundance water. FIDs, free induction decays; PIN, a positive-intrinsic-negative; TR, repetition time.

administered within 2 min after 5-min baseline acquisition of interleaved ^{2}H–^{17}O spectra. Each rat underwent two consecutive inhalations of $^{17}O_2$ gas (74.8% enrichment, Sigma-Aldrich, mixed with N_2O and isoflurane), each lasting approximately 2 min, occurring during and 30 min after the D66 glucose administration.

After B_0 shimming and ^{1}H MRI acquisition, dynamic ^{17}O–^{2}H MRS data from the rat brains were acquired for 80 min using the same interleaved ^{2}H–^{17}O MRS pulse-acquire sequence (Figure 3A) and parameters as described above. The ^{2}H–^{17}O FID data underwent 15-Hz line broadening before Fourier transformation to enhance the SNR. A custom Matlab-based program was employed to fit all resonance signals, and the resulting spectral integrals were used to quantify the metabolite concentrations after correcting the saturation effects (for ^{2}H spectra). The natural

abundance ^{17}O or ^{2}H water signal acquired in the brain at the baseline condition served as an internal reference for quantification of metabolite concentration.[6,8]

2.5 | Kinetic models and quantification

For an aerobic organ with a higher oxygen metabolic rate and blood perfusion (such as the brain or heart), the detected ^{17}O MRS signal of brain tissue $H_2{}^{17}O$ and its time-dependent change can be characterized by three phases as shown in Figure S1, and the modeling and quantification can be significantly simplified for rodents with a relatively small body size and a short $^{17}O_2$ inhalation as previously described[8,24,25]:

1. Phase I (pre-inhalation): stable natural abundance ^{17}O MRS signal of brain tissue $H_2{}^{17}O$, which can be used as an internal reference for quantifying tissue $H_2{}^{17}O$ concentration and its change measured in later phases
2. Phase II ($^{17}O_2$ inhalation): ^{17}O MRS signal during a brief $^{17}O_2$ inhalation (usually lasting a few minutes), showing a rapid increase in brain tissue $H_2{}^{17}O$ content through the metabolism of inhaled $^{17}O_2$ in brain cells; the dynamic $H_2{}^{17}O$ signal change can be used to quantify $CMRO_2$
3. Phase III (post-inhalation): ^{17}O MRS signal after the $^{17}O_2$ inhalation, where the labeled $H_2{}^{17}O$ molecules produced by the metabolism of inhaled $^{17}O_2$ in the brain tissue can be washed out via blood perfusion; the $H_2{}^{17}O$ signal can be used as an endogenous perfusion tracer to measure and quantify CBF

The mass balance relationship for the changes in the labeled $H_2{}^{17}O$ concentration in different tissue compartments during an $^{17}O_2$ gas inhalation is given by Equation (1)[8,24]:

$$\frac{dC_b(t)}{dt} = 2\cdot\alpha\cdot f_1\cdot CMRO_2 + f_2\cdot CBF[C_a(t) - C_v(t)], \tag{1}$$

where C_a, C_b, and C_v are the $H_2{}^{17}O$ concentrations expressed in excess of the natural abundance $H_2{}^{17}O$ level in arterial blood, brain tissue, and venous blood, respectively, as a function of the $^{17}O_2$ inhalation time t (unit = minute). One labeled $^{17}O_2$ molecule converts to two $H_2{}^{17}O$ molecules through oxygen metabolism; thus, a constant of 2 is used in Equation (1). The parameter α in Equation (1) is the ^{17}O enrichment fraction in the inhaled $^{17}O_2$ gas. The natural abundance $H_2{}^{17}O$ concentration (equal to 20.4 μmol per gram of tissue water or per gram of water in blood; see references 8 and 24) can be used to calibrate the absolute concentrations of $C_b(t)$, $C_a(t)$, and $C_v(t)$. For convenience, the unit for C_b is chosen as micromoles per gram of brain tissue water and the units for C_a and C_v are micromoles per gram of blood water, and the parameters f_1 (=1.266) and f_2 (=1.077) are conversion factors used for consistency of units applied in Equation (1).[8,24]

For in vivo ^{17}O MRS brain application in rodents, which have smaller bodies and rapid pulmonary gas exchange, the contributions of blood recirculation (i.e., the C_a term in Equation (1)) and blood washout via perfusion (i.e., the C_v term in Equation (1)) during a short $^{17}O_2$ gas inhalation (e.g., 2–3 min) are similar, so the second term on the right-hand side of Equation (1) becomes negligible, and this approximation leads to a linear differential equation[8,24]:

$$CMRO_2 \approx \frac{dC_b(t)}{dt}\cdot\frac{1}{2\cdot\alpha\cdot f_1}, \tag{2}$$

where the $dC_b(t)/dt$ term represents the slope of the brain tissue $H_2{}^{17}O$ concentration (i.e., $[H_2{}^{17}O]$) change in phase II, and it can be determined by linear regression.

During phase III, the dynamic $[H_2{}^{17}O]$ change reflects the perfusion process in the brain tissue according to an exponential decay (measurable by the decay rate constant k) and can be used to estimate the CBF value according to Equation (3)[5,26]:

$$CBF \approx 1.86\times k, \tag{3}$$

where the constant k is determined by fitting the post-inhalation $C_b(t)$ time course to an exponential function.[5,26,27] The OEF value can be determined from the corresponding $CMRO_2$ and CBF values according to Equation (4)[27]:

$$OEF = \frac{CMRO_2}{C_{a,O_2}\times CBF}, \tag{4}$$

where C_{a,O_2} is the arterial oxygen concentration, assumed constant at 18 mL O_2/dL blood (equivalent to 18/2.24 μmol/mL blood). Note that the simplified models as described by Equations (2) and (3) provide good approximations for rodent brain application. However, they are not applicable to the human brain owing to a much larger body size and much slower pulmonary gas exchange process; thus, both oxygen metabolism and perfusion processes can contribute to the dynamic [$H_2{}^{17}O$] changes in phases II and III, and a sophisticated quantification model is needed.[28–30]

For in vivo ^2H MRS application in rat brains, the original kinetic model does not include the glycolysis pathway and CMR_{Lac} owing to a low level of ^2H-labeled lactate in healthy rat brains.[6] In this study, we modified the previous kinetic model[6] by replacing the glycogen pathway with the lactate formation pathway as illustrated in Figure S2. Using the modified kinetic model and the arterial blood input functions reported in our early rat brain work using the same D66 infusion protocol and anesthesia condition (2% isoflurane),[6] we estimated three key cerebral metabolic rates: CMR_{Glc}, CMR_{Lac}, and V_{TCA}. This involved fitting the concentration time courses of deuterated metabolites (glucose, lactate, and the combined glutamate/glutamine: Glx) to the modified kinetic model (Figure S2).

Ultimately, through a single dynamic interleaved ^2H–^{17}O MRS measurement, six key physiological parameters, $CMRO_2$, CBF, OEF, CMR_{Glc}, V_{TCA}, and CMR_{Lac}, were simultaneously measured and determined.

3 | RESULTS

3.1 | RF coil design, prototype, and bench test

Figure 2A illustrates the circuit layout of the newly designed RF surface coil that can be operated at $^1H/^2H/^{17}O$ triple resonant frequencies. Figure 2B displays the prototype of this coil. Figure 2C presents the S11 measurement outcomes for the prototype coil when it was tested under the heavy loading condition using a large water phantom. The RF coil quality (Q) factors, derived from the S11 parameters under the loaded condition, were calculated to be 23.3 for the ^1H resonant frequency, 20.6 for the ^2H resonant frequency, and 20.6 for ^{17}O resonant frequency.

3.2 | Design of the interleaved ^2H–^{17}O MRS pulse sequence and phantom validation

Figure 3A depicts a schematic of a modified single-pulse acquisition (SPULS) sequence used to collect five ^{17}O FIDs followed by one ^2H FID in an interleaved way for each element and then repeated 20 times for signal averaging. In this configuration, the TR for acquiring ^{17}O signals was set to 50 ms; however, as the ^{17}O MRS acquisition was repeated five times, the effective TR of ^2H was 300 ms ($=6 \times 50$ ms). The total acquisition count for acquiring the interleaved ^2H–^{17}O MRS was set to 20, yielding a temporal resolution of 6 s for the phantom test. This count can be adjusted to accommodate different experimental designs or SNR requirements. ^2H FIDs were acquired when the PIN diode was reverse-biased in an off state and the RF hard pulse was set to the ^2H Larmor frequency (107 MHz at 16.4 T) with an Ernst FA, whereas ^{17}O FIDs were collected when the PIN diode was forward-biased in an on state and the RF hard pulse was set to the ^{17}O Larmor frequency (94 MHz at 16.4 T) with a nominal 90° FA. Figure 3B illustrates a series of water spectra acquired from a phantom using the interleaved ^2H–^{17}O MRS pulse sequence (Figure 3A), with the upper panel (black lines) showing the ^2H spectra of naturally abundant HDO and the lower panel (red lines) showing the ^{17}O spectra of naturally abundant $H_2{}^{17}O$ from the water phantom. The ^2H signal exhibited greater fluctuation compared with the ^{17}O signal, which was acquired under full relaxation conditions and had a signal average five times greater than that of the ^2H signal, thus a better SNR and a smaller fluctuation. Figure 3C displays the ^1H MRI of a spherical water phantom in three orientations. Figure 3D compares the averaged ^2H and ^{17}O water resonance spectra acquired in an interleaved manner with those acquired individually in the conventional manner (i.e., the control). The well-matched control and interleaved spectra of ^2H and ^{17}O confirm the excellent performance of the multifrequency surface coil and the modified pulse sequence. Additionally, to prevent mixing up of the ^2H and ^{17}O water signals in the interleaved scans, we intentionally shifted the ^{17}O water signal in the receiver frequency by approximately 400 Hz.

3.3 | Rat brain experiment with bolus injection of D_2O and $H_2{}^{17}O$

Figure 4A,B shows the results of the dynamic ^2H–^{17}O MRS measurements before, during, and after the concurrent intravenous injection of D_2O and $H_2{}^{17}O$ tracers. The stack plots depict the HDO and $H_2{}^{17}O$ spectra, presenting averaged labeled water signals with a temporal resolution of 1 min per spectrum. Exponential fitting of the post-injection water signals yields decay rate constant (k) values of 0.37 and 0.38 min^{-1} for HDO and $H_2{}^{17}O$ measurements, respectively, reflecting the perfusion process in the rat brain. Although the HDO signal intensity is significantly higher than that of $H_2{}^{17}O$ due to the higher deuterium enrichment (or dose) of the D_2O tracer, the measured decay rate constants of the HDO and $H_2{}^{17}O$ signals are almost identical as anticipated. Note that the accurate quantification of the actual CBF values ideally requires the blood input functions after the infusion of tracers, which were not measured in this study.

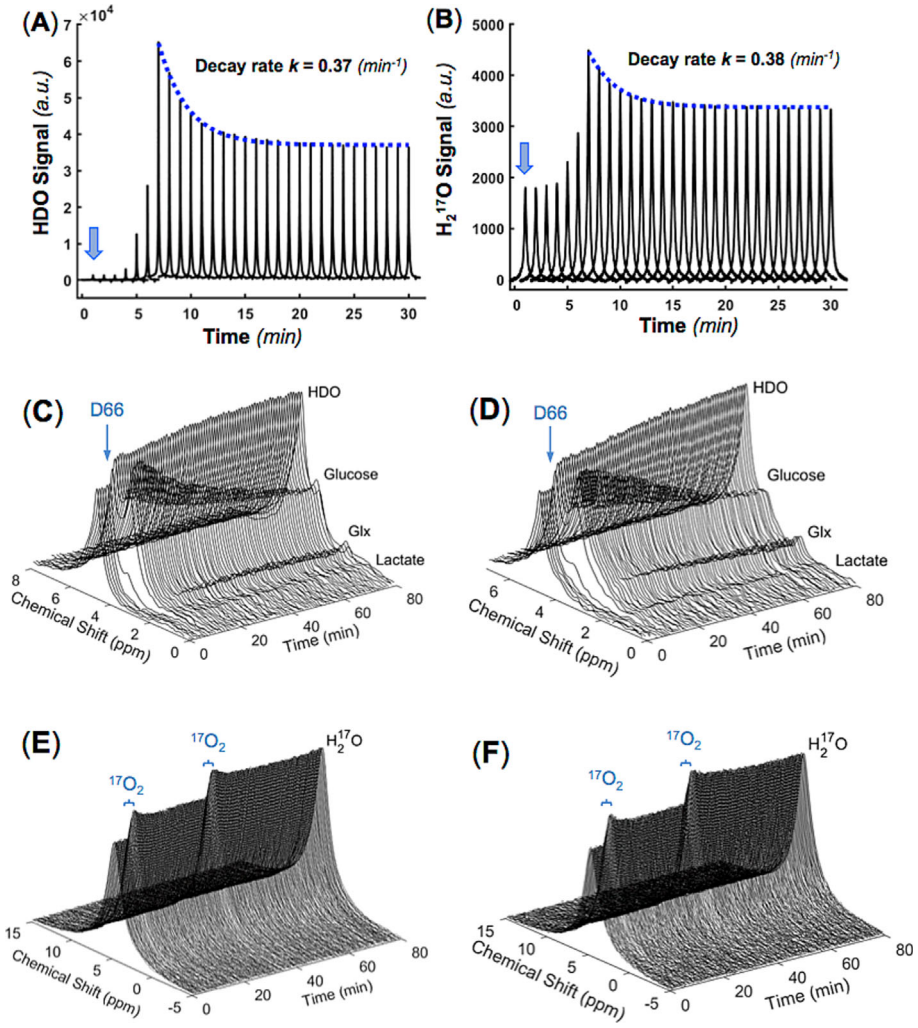

FIGURE 4 Dynamic ^{2}H and ^{17}O MRS results obtained from a rat brain during a 6-min intravenous infusion of D_2O and $H_2{}^{17}O$ water, with the onset of infusion indicated by the blue arrows. The dynamic spectra of averaged HDO (A) and $H_2{}^{17}O$ (B) resonance signals are presented at a temporal resolution of 1 min per spectrum. The decay rate constants (k) for the post-infusion HDO and $H_2{}^{17}O$ signals were determined as 0.37 and 0.38 min^{-1}, respectively. Stack plots of the dynamic brain ^{2}H spectra (C, D) and ^{17}O spectra (E, F) acquired continuously over 80 min in two rats (C, E for rat A and D, F for rat B), undergoing simultaneous intravenous administration of D66 glucose and inhalation of $^{17}O_2$ gas at 5–7 min, followed by another $^{17}O_2$ gas inhalation at 35–37 min.

3.4 | Rat brain experiments with D66 glucose administration and $^{17}O_2$ gas inhalation

Two rats used in this experiment exhibited some differences in their BW, end tidal CO_2 ($EtCO_2$), and body temperature (T): BW = 335 g, $EtCO_2 \approx 2.7\%–3.0\%$, and $T \approx 38.0–38.2°C$ for rat A and BW = 254 g, $EtCO_2 \approx 3.5\%–3.8\%$, and $T \approx 38.6–38.8°C$ for rat B. The stack plots of the dynamic brain ^{2}H and ^{17}O spectra obtained during the 80-min interleaved $^{2}H–^{17}O$ MRS data acquisition in two rats are shown in Figure 4C–F. Both rats underwent simultaneous D66 glucose intravenous administration and $^{17}O_2$ gas inhalation after 5-min baseline acquisition and a subsequent $^{17}O_2$ gas inhalation 30 min after the D66 glucose injection. The quality of the $^{2}H–^{17}O$ spectra and the dynamic changes in the ^{17}O-labeled water ($H_2{}^{17}O$) signal and ^{2}H-labeled water (HDO), glucose (Glc), mixed glutamate and glutamine (Glx), and lactate (Lac) signals are clearly captured and demonstrated herein. Subsequent data analysis yielded concentration (presented in millimolar unit) time courses of $H_2{}^{17}O$ with $^{17}O_2$ inhalations as measured by ^{17}O MRS (Figure 5), as well as Glc, Glx, and Lac after an intravenous infusion of deuterium-labeled glucose as measured by ^{2}H MRS (Figure 6), and they were utilized in model fitting to estimate the relevant physiology parameters of interest.

$CMRO_2$ and CBF values were calculated by regression of the brain [$H_2{}^{17}O$] time courses according to Equations (2) and (3), respectively, as summarized in Figure 5, showing moderately higher CBF values in rat A (0.83 and 0.54 mL/g/min for the first and second measurements) than in rat B (0.66 and 0.37 mL/g/min) and slightly lower $CMRO_2$ values in rat A (1.26 and 1.19 μmol/g/min) than in rat B (1.36 and 1.24 μmol/g/min). Interestingly, both rats exhibited a decrease in CBF (34.9% in rat A and 43.9% in rat B) and a smaller reduction in $CMRO_2$ (5.6% in rat A and 8.8%

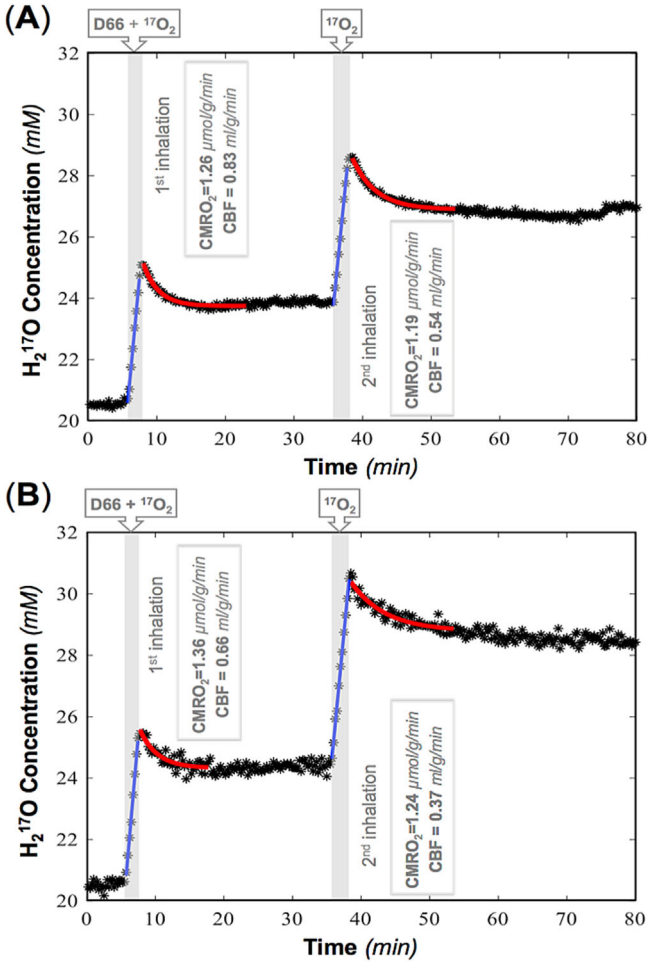

FIGURE 5 Time courses and model regressions of brain tissue $H_2{}^{17}O$ concentration and the corresponding cerebral blood flow (CBF) and cerebral metabolic rate of oxygen consumption ($CMRO_2$) values for two rats ((A) rat A and (B) rat B) during two repeated $^{17}O_2$ inhalations. The shaded areas indicate the durations of $^{17}O_2$ inhalation, and the blue and red lines depict the linear and exponential fittings of the experimental data (star symbols) used to calculate the $CMRO_2$ and CBF values according to Equations (2) and (3), respectively. D66, D-glucose-6,6-d_2.

in rat B) about 30 min after D66 administration, suggesting a potential hyperglycemia effect of glucose administration or a potential decline in animal physiology condition. Nevertheless, further investigation is necessary to confirm this observation. The averaged OEF was 0.28 in rat A, significantly lower than the OEF of 0.40 in rat B, which may be due to their different physiological conditions. The relatively low (global) $CMRO_2$ values observed in this study can be attributed to the partial volume effect caused by the large RF coil size relative to the rat brain, resulting in significant contamination from surrounding tissues such as muscle with several times low metabolic activity.[30]

Figure 6 displays the concentration dynamics of deuterated metabolites fitted to the modified kinetic model (Figure S2), demonstrating excellent fitting quality. The derived values of CMR_{Glc} and V_{TCA} were similar between rat A (0.60 and 1.16 μmol/g/min, respectively) and rat B (0.67 and 1.17 μmol/g/min, respectively), although rat B showed a higher CMR_{Lac} value compared with rat A (0.17 μmol/g/min vs. 0.05 μmol/g/min for rat A) and a higher Glx turnover.

Table 1 summarizes all quantified physiological parameters from two rats with mean values of $CMRO_2$ = 1.26 μmol/g/min, CBF = 0.60 mL/g/min, OEF = 0.34, CMR_{Glc} = 0.64 μmol/g/min, V_{TCA} = 1.17 μmol/g/min, and CMR_{Lac} = 0.11 μmol/g/min. These values are in general consistent with the literature reports (e.g., in the reference[31]).

4 | DISCUSSION

In a normal brain, most glucoses are metabolized through mitochondrial oxidative pathways to meet the high ATP energy demand required for various cellular activities and brain functions while maintaining ATP homeostasis. However, altered brain states may trigger metabolic reprogramming, leading to significant changes in the relative contribution of glycolysis to overall energy production.[32–36] It is widely recognized that

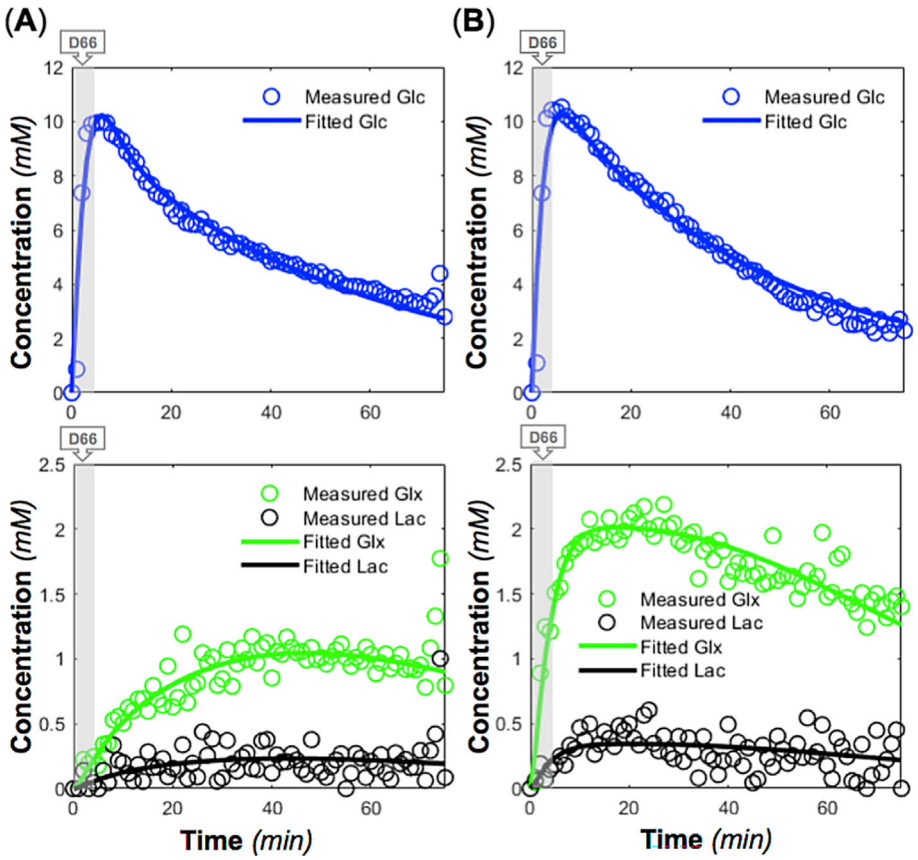

FIGURE 6 Time courses and model fittings of brain deuterated glucose (Glc), glutamate/glutamine (Glx), and lactate (lac) concentrations in two rats ((A) rat A and (B) rat B) during and after D-glucose-6,6-d_2 (D66) administration (indicated by shaded areas) using the modified kinetic model (Figure S2). The derived cerebral metabolic rate of glucose consumption (CMR_{Glc}), cerebral metabolic rate of the tricarboxylic acid cycle (V_{TCA}), and cerebral metabolic rate of lactate formation (CMR_{Lac}) values from the model fitting were 0.60, 1.16, and 0.05 μmol/g/min for rat A and 0.67, 1.17, and 0.17 μmol/g/min for rat B, respectively.

TABLE 1 Summary of measured rat brain metabolic rates, cerebral blood flow (CBF), and oxygen extraction fraction (OEF) results.

Rat	$CMRO_2$ (μmol/g/min)	CBF (mL/g/min)	OEF	CMR_{Glc} (μmol/g/min)	V_{TCA} (μmol/g/min)	CMR_{Lac} (μmol/g/min)
A	1.26	0.83	0.28	0.60	1.16	0.05
	1.19	0.54				
B	1.36	0.66	0.40	0.67	1.17	0.17
	1.24	0.37				
Average	1.26	0.60	0.34	0.64	1.17	0.11

brain cancer cells exhibit a significant increase in lactate production under aerobic conditions, a process known as the "Warburg effect."[27,32,37–39] Furthermore, changes in aerobic glycolysis are implicated in various brain disorders, including Alzheimer's disease and other neurodegenerative conditions.[39–46] Interestingly, even in the healthy human brain, aerobic glycolysis is also enhanced in the human visual cortex during visual stimulation with a sufficient cellular oxygen level, resulting in an elevation in lactate and much large increases in CMR_{Glc} and CBF than $CMRO_2$.[34,47–49] Such a metabolic shift or enhanced aerobic glycolysis plays a crucial role in synaptic plasticity and adaptation learning[35,36] as well as brain development,[50] and conversely, the contribution of aerobic glycolysis decreases with age at varied paces in different brain regions.[50,51] The ample evidence highlights the fundamental role of metabolic reprogramming in healthy and diseased brains.[47,52] Therefore, it is imperative to develop in vivo MRS and imaging techniques that can simultaneously measure and quantify the cerebral glucose and oxygen metabolic rates as well as blood flow.

In this work, we developed a novel RF surface coil approach based on a dual-frequency coil design[20] and a circuit controller[21] that enables ^{1}H MRI and interleaved ^{2}H–^{17}O MRS measurements. This design creates two primary resonant circuits in the same loop coil that cover a wide tuning range from the ^{1}H frequency of 698 MHz to the ^{17}O or ^{2}H frequency of 94 or 107 MHz at 16.4 T. This approach offers a simple and cost-

effective RF coil solution that overcomes prevalent challenges in multi-nuclei MRI/MRS imaging and RF coil design, ensuring adequate detection sensitivity for ^{1}H MRI and achieving excellent performance for low-γ X-nuclear MRS imaging (e.g., ^{17}O and ^{2}H) as the single-frequency surface coil with the same coil size and geometry.[20] Essentially, this coil design allows the measurement of multiple low-γ X-nuclei, such as ^{2}H and ^{17}O, within the tuning range. However, in practical applications, the transition between different nuclear spins or operation frequencies requires manual adjustment. To address this issue and enable rapid and active tuning and retuning, a PIN-diode circuit was integrated into the dual-frequency coil design to facilitate the active switching between the ^{2}H and ^{17}O operation frequencies (Figure 2). This integration makes interleaved in vivo ^{2}H and ^{17}O measurements possible. The PIN diode acts as a nonlinear, current-controlled resistor at the desired RFs, providing a resistance of 0.1–0.5 Ω in forward bias, effectively creating a short circuit for the RF current and increasing to several kiloohms in reverse bias, resulting in an open circuit.[53] This property makes PIN diodes important components in transmit–receive (T/R) coils and switches and enables rapid switching between different resonant frequencies in multifrequency coils.[54–56] It is particularly useful when switching between nuclei with closely spaced resonant frequencies by adding extra parallel tuning and matching capacitance (controlled by PIN didoes), as illustrated in Figure 2A.[57] Our current coil design is specifically optimized for active frequency switching between ^{2}H and ^{17}O at 16.4 T, given the proximity of their resonant frequencies (13 MHz apart) and their alignment within the tuning range suited for the low-γ resonant frequencies.

The performance of the novel RF surface coil was evaluated through phantom testing to detect natural abundance HDO and $H_2{}^{17}O$ water signals, as well as through a rat brain perfusion experiment. The latter utilized dynamic ^{2}H–^{17}O MRS measurements with simultaneous administration of D_2O and $H_2{}^{17}O$ dual tracers. The analysis revealed that the decay rate constants regressed from the interleaved ^{2}H and ^{17}O data sets are nearly identical, although that the intensity of the HDO signal was significantly higher than that of $H_2{}^{17}O$ due to the higher dose of deuterium label introduced into the same brain (see Figure 4A,B). This is expected because the decay rate reflects brain tissue perfusion and should be independent of the dose of tracer used.

$CMRO_2$, CBF, and OEF are three important parameters for evaluating cerebral oxygen metabolism and perfusion and the coupling between them, which can be determined by ^{17}O MRS or imaging.[8,26,58] Likewise, CMR_{Glc}, CMR_{Lac}, and V_{TCA} are critical for the assessment of cerebral glucose metabolism along major metabolic pathways and can be measured by the recently developed in vivo ^{2}H MRS or imaging technique.[6] The method developed in this work enables simultaneous determination of those six parameters, making it possible for the first time to perform a comprehensive and quantitative assessment of cerebral glucose and oxygen metabolism and perfusion from a single dynamic measurement, as demonstrated in Figures 4–6.

Although the novel RF coil and associated MRS acquisition and quantification methods described herein allow simultaneous and quantitative assessment of rat brain glucose and oxygen metabolism and perfusion at 16.4 T, the current study is limited by using only surface coil localization. The in vivo ^{2}H and ^{17}O MRS signals obtained using the RF coil (2.5-cm diameter, Figure 2B) and the modified SPULS sequence (Figure 3A) should originate mainly from the rat brain; however, there is significant contamination from the surrounding muscle with lower metabolic activity, so the values reported in Table 1 may be affected by the partial volume effect. In particular, contamination may lead to an underestimation of $CMRO_2$ due to the significant effect of the recirculating $H_2{}^{17}O$ into the brain and surrounding tissues. Nevertheless, this may be less critical for measuring other metabolic rates based on the labeled metabolites (e.g., Glx), which remains primarily within the brain cells and absent in the surrounding muscle. Technical limitations of this study precluded imaging of the six parameters in different brain regions. Nonetheless, the interleaved ^{2}H–^{17}O single-pulse acquisition sequence can be extended to a three-dimensional (3D) interleaved ^{2}H–^{17}O chemical shift imaging (CSI) theme by adding phase encoding and dephasing gradients, for instance, as illustrated in Figure S3. Advanced post-processing and denoising techniques can also be applied to the 3D CSI data to further improve SNR and achieve high-resolution metabolic mapping of rodent brains.[59,60] Additionally, the interleaved ^{2}H–^{17}O MRS or imaging method could be adapted for human brain applications, which requires new hardware such as RF coils or coil arrays customized for the human brain imaging, or could be employed for a relatively lower field strength potentially for translational or clinical applications (e.g., at 3 T) with a decent imaging resolution.[61,62]

Although the measured metabolic rates and perfusion parameters in this study are within the ranges as reported in the literature, there are some limitations beside surface coil localization as discussed above. First, the dual-perfusion tracers (HDO and $^{17}H_2O$) were injected into the body via the femoral vein rather than the internal carotid artery as reported in our early studies,[8,16] invariably involving tracer dilation in the heart and lung. Therefore, the measured decay rate constants as shown in Figure 4A,B are not accurate for directly determining the true CBF values, and additional information about blood input function is needed. Second, the blood input functions related to the total and deuterium-labeled glucoses in blood were not measured during the dynamic measurements of interleaved ^{2}H–^{17}O MRS in this study; therefore, the reported CMR_{Glc}, CMR_{Lac}, and V_{TCA} values present approximated estimations. Finally, the number of animals used for this study was small and it limits the accuracy of the measurement and derived values. More studies are needed.

5 | CONCLUSIONS

To address the technical hurdles of using ^{2}H and ^{17}O MRS technologies to simultaneously study cerebral glucose and oxygen metabolism and perfusion, we developed a novel surface coil paired with a modified pulse sequence and a circuit controller to achieve active switching between the ^{2}H

and ^{17}O Larmor frequencies. With this capability, our study marks the first time that interleaved ^{2}H–^{17}O MRS technology combined with concurrent ^{2}H-labeled glucose administration and ^{17}O-labeled oxygen gas inhalation can simultaneously measure and quantify six key metabolic and perfusion parameters (CMR_{Glc}, CMR_{Lac}, $CMRO_2$, V_{TCA}, CBF, and OEF) in a single dynamic scan. This method not only saves scanning time but also improves measurement accuracy by minimizing variations associated with changes in the animal's condition commonly across multiple measurements. Looking forward, further developments, such as incorporating spatial localization or imaging capabilities, could greatly expand the utility of this technology in a wide range of biomedical applications, especially in exploring brain energy metabolism, metabolic reprograming, and their interplay with cerebral perfusion in healthy brains and aging-related changes and more importantly in many disordered brains, including tumor, stroke, and neurovegetative diseases. Finally, the same interleaved ^{2}H–^{17}O MRS or imaging technology can be also applied to other organs or different field strengths.

AUTHOR CONTRIBUTIONS

Wei Chen and Xiao-Hong Zhu designed the study; Guangle Zhang, Wei Zhu, and Xiao-Hong Zhu conducted the study; Parker Jenkins built the RF coil and circuit; Guangle Zhang analyzed the data; and Guangle Zhang, Wei Chen, and Xiao-Hong Zhu wrote the manuscript.

ACKNOWLEDGMENTS

This work was supported in part by National Institutes of Health (NIH) grants R01 MH111413, R01 NS133006, R01 CA240953, S10 RR025031, and P41 EB027061.

CONFLICT OF INTEREST STATEMENT

The authors declare no potential conflicts of interest with respect to the research, authorship, and/or publication of this article.

DATA AVAILABILITY STATEMENT

The data that support the findings of this study are available from the corresponding author upon reasonable request.

SUPPORTING INFORMATION

The supporting information for this article is available online.

ORCID

Wei Chen https://orcid.org/0000-0002-9608-1444

REFERENCES

1. Mergenthaler P, Lindauer U, Dienel GA, Meisel A. Sugar for the brain: the role of glucose in physiological and pathological brain function. *Trends Neurosci*. 2013;36(10):587-597. doi:10.1016/j.tins.2013.07.001
2. Zhu X-H, Lu M, Chen W. Quantitative imaging of brain energy metabolisms and neuroenergetics using *in vivo* X-nuclear ^{2}H, ^{17}O and ^{31}P MRS at ultra-high field. *J Magn Reson*. 2018;292:155-170. doi:10.1016/j.jmr.2018.05.005
3. Siesjo BK. *Brain Energy Metabolism*. (Wiley; 1978:101-110).
4. Clarke DD, Sokoloff L. Circulation and energy metabolism of the brain. In: Siegel GJ et al., eds. *Basic Neruochemistry: Molecular, Cellular and Medical Aspects*. (Lippincott-Raven Publishers; 1999:633-669.
5. Zhu X-H, Zhang N, Zhang Y, Zhang X, Ugurbil K, Chen W. *In vivo* ^{17}O NMR approaches for brain study at high field. *NMR Biomed*. 2005;18(2):83-103. doi:10.1002/nbm.930
6. Lu M, Zhu X-H, Zhang Y, Mateescu G, Chen W. Quantitative assessment of brain glucose metabolic rates using in vivo deuterium magnetic resonance spectroscopy. *J Cereb Blood Flow Metab*. 2017;37(11):3518-3530. doi:10.1177/0271678X17706444
7. De Feyter HM, Behar KL, Corbin ZA, et al. Deuterium metabolic imaging (DMI) for MRI-based 3D mapping of metabolism in vivo. *Sci Adv*. 2018;4(8):eaat7314. doi:10.1126/sciadv.aat7314
8. Zhu X-H, Zhang Y, Tian R-X, et al. Development of ^{17}O NMR approach for fast imaging of cerebral metabolic rate of oxygen in rat brain at high field. *Proc Natl Acad Sci*. 2002;99(20):13194-13199. doi:10.1073/pnas.202471399
9. Gruetter R, Novotny EJ, Boulware SD, et al. Direct measurement of brain glucose concentrations in humans by ^{13}C NMR spectroscopy. *Proc Natl Acad Sci U S a*. 1992;89(3):1109-1112. doi:10.1073/pnas.89.3.1109
10. Lu M, Zhang Y, Ugurbil K, Chen W, Zhu XH. *In vitro* and *in vivo* studies of ^{17}O NMR sensitivity at 9.4 and 16.4 T. *Magn Reson Med*. 2013;69(6):1523-1527. doi:10.1002/mrm.24386
11. Lu M, Chen W, Zhu XH. Field dependence study of *in vivo* brain ^{31}P MRS up to 16.4 T. *NMR Biomed*. 2014;27(9):1135-1141. doi:10.1002/nbm.3167
12. de Graaf RA, Hendriks AD, Klomp DW, et al. On the magnetic field dependence of deuterium metabolic imaging. *NMR Biomed*. 2020;33(3):e4235. doi:10.1002/nbm.4235
13. Alecci M, Romanzetti S, Kaffanke J, Celik A, Wegener HP, Shah NJ. Practical design of a 4 tesla double-tuned RF surface coil for interleaved ^{1}H and ^{23}Na MRI of rat brain. *J Magn Reson*. 2006;181(2):203-211. doi:10.1016/j.jmr.2006.04.011
14. Kan S, Fan M, Courtieu J. A single-coil triple resonance probe for NMR experiments. *Rev Sci Instrum*. 1980;51(7):887-890. doi:10.1063/1.1136352
15. Schnall M, Subramanian VH, Leigh J Jr, Chance B. A new double-tuned probed for concurrent ^{1}H and ^{31}P NMR. *J Magn Reson*. 1969;1985(65):122-129. doi:10.1016/0022-2364(85)90380-4

16. Zhu XH, Merkle H, Kwag JH, Ugurbil K, Chen W. ^{17}O relaxation time and NMR sensitivity of cerebral water and their field dependence. *Magn Reson Med*. 2001;45(4):543-549. doi:10.1002/mrm.1073
17. Pang Y, Xie Z, Xu D, et al. A dual-tuned quadrature volume coil with mixed λ/2 and λ/4 microstrip resonators for multinuclear MRSI at 7 T. *Magn Reson Imaging*. 2012;30(2):290-298. doi:10.1016/j.mri.2011.09.022
18. Yan X, Xue R, Zhang X. A monopole/loop dual-tuned RF coil for ultrahigh field MRI. *Quant Imaging Med Surg*. 2014;4:225.
19. Rutledge O, Kwak T, Cao P, Zhang X. Design and test of a double-nuclear RF coil for ^{1}H MRI and ^{13}C MRSI at 7T. *J Magn Reson*. 2016;267:15-21. doi:10.1016/j.jmr.2016.04.001
20. Zhang G, Zhu W, Li X, Zhu XH, Chen W. Dual-frequency resonant coil design for low-γ X-nuclear and proton magnetic resonance imaging at ultrahigh field. *NMR Biomed*. 2023;36(8):e4930. doi:10.1002/nbm.4930
21. Jenkins P, Zhang G, Zhu W, Zhu XH, Chen W. Single loop tri-frequency surface coil design for ^{1}H MRI and interleaved dynamic ^{2}H and ^{17}O MRS applications at ultrahigh field of 16.4T. In: *Proc. Intl. Soc. Mag. Reson. Med*. Vol.29; 2021:1816.
22. Ackerman JJ, Ewy CS, Becker NN, Shalwitz RA. Deuterium nuclear magnetic resonance measurements of blood flow and tissue perfusion employing 2H2O as a freely diffusible tracer. *Proc Natl Acad Sci U S a*. 1987;84(12):4099-4102. doi:10.1073/pnas.84.12.4099
23. Mispelter JI, Lupu M, Briguet A. *NMR probeheads for biophysical and biomedical experiments: theoretical principles and practical guidelines*. Imperial College Press; 2006. doi:10.1142/p438
24. Zhang N, Zhu XH, Lei H, Ugurbil K, Chen W. Simplified methods for calculating cerebral metabolic rate of oxygen based on ^{17}O magnetic resonance spectroscopic imaging measurement during a short $^{17}O_2$ inhalation. *J Cereb Blood Flow Metab*. 2004;24(8):840-848. doi:10.1097/01.WCB.0000125885.54676.82
25. Zhu XH, Chen W. Quantitative ^{17}O MRSI of myocardial oxygen metabolic rate, blood flow, and oxygen extraction fraction under normal and high workload conditions. *Magn Reson Med*. 2024;91(4):1645-1658. doi:10.1002/mrm.29908
26. Zhu XH, Zhang Y, Wiesner HM, Ugurbil K, Chen W. *In vivo* measurement of CBF using ^{17}O NMR signal of metabolically produced $H_2{}^{17}O$ as a perfusion tracer. *Magn Reson Med*. 2013;70(2):309-314. doi:10.1002/mrm.24469
27. Zhu XH, Chen JM, Tu TW, Chen W, Song SK. Simultaneous and noninvasive imaging of cerebral oxygen metabolic rate, blood flow and oxygen extraction fraction in stroke mice. *Neuroimage*. 2013;64:437-447. doi:10.1016/j.neuroimage.2012.09.028
28. Atkinson IC, Thulborn KR. Feasibility of mapping the tissue mass corrected bioscale of cerebral metabolic rate of oxygen consumption using 17-oxygen and 23-sodium MR imaging in a human brain at 9.4 T. *Neuroimage*. 2010;51(2):723-733. doi:10.1016/j.neuroimage.2010.02.056
29. Zhu XH, Wiesner HM, Lee BY, Lu M, Chen W. Quantitative and simultaneous imaging of $CMRO_2$, CBF and OEF in resting human brain. In: *Proc. Intl. Soc. Mag. Reson. Med*. Vol.23; 2015:895.
30. Wiesner HM, Balla DZ, Scheffler K, et al. Quantitative and simultaneous measurement of oxygen consumption rates in rat brain and skeletal muscle using ^{17}O MRS imaging at 16.4T. *Magn Reson Med*. 2021;85(4):2232-2246. doi:10.1002/mrm.28552
31. Wood TC, Cash D, MacNicol E, et al. Non-invasive measurement of the cerebral metabolic rate of oxygen using MRI in rodents. *Wellcome Open Res*. 2021;6:109. doi:10.12688/wellcomeopenres.16734.2
32. Heiden MGV, Cantley LC, Thompson CB. Understanding the Warburg effect: the metabolic requirements of cell proliferation. *Science*. 2009;324(5930):1029-1033. doi:10.1126/science.1160809
33. Barinaga M. What makes brain neurons run? *Science*. 1997;276(5310):196-198. doi:10.1126/science.276.5310.196
34. Li H, Guglielmetti C, Sei YJ, et al. Neurons require glucose uptake and glycolysis in vivo. *Cell Rep*. 2023;42(4):112335. doi:10.1016/j.celrep.2023.112335
35. Magistretti PJ. Imaging brain aerobic glycolysis as a marker of synaptic plasticity. *Proc Natl Acad Sci U S a*. 2016;113(26):7015-7016. doi:10.1073/pnas.1607423113
36. Shannon BJ, Vaishnavi SN, Vlassenko AG, Shimony JS, Rutlin J, Raichle ME. Brain aerobic glycolysis and motor adaptation learning. *Proc Natl Acad Sci U S a*. 2016;113(26):E3782-E3791. doi:10.1073/pnas.1604977113
37. Warburg O. On the origin of cancer cells. *Science*. 1956;123(3191):309-314. doi:10.1126/science.123.3191.309
38. Faubert B, Solmonson A, DeBerardinis RJ. Metabolic reprogramming and cancer progression. *Science*. 2020;368(6487):eaaw5473. doi:10.1126/science.aaw5473
39. Ward PS, Thompson CB. Metabolic reprogramming: a cancer hallmark even Warburg did not anticipate. *Cancer Cell*. 2012;21(3):297-308. doi:10.1016/j.ccr.2012.02.014
40. Goyal MS, Blazey T, Metcalf NV, et al. Brain aerobic glycolysis and resilience in Alzheimer disease. *Proc Natl Acad Sci U S a*. 2023;120(7):e2212256120. doi:10.1073/pnas.2212256120
41. Harris RA, Tindale L, Cumming RC. Age-dependent metabolic dysregulation in cancer and Alzheimer's disease. *Biogerontology*. 2014;15(6):559-577. doi:10.1007/s10522-014-9534-z
42. Vlassenko AG, Raichle ME. Brain aerobic glycolysis functions and Alzheimer's disease. *Clin Transl Imaging*. 2015;3(1):27-37. doi:10.1007/s40336-014-0094-7
43. Hanahan D, Weinberg RA. Hallmarks of cancer: the next generation. *Cell*. 2011;144(5):646-674. doi:10.1016/j.cell.2011.02.013
44. Calsolaro V, Edison P. Alterations in glucose metabolism in Alzheimer's disease. *Recent Pat Endocr Metab Immune Drug Discov*. 2016;10(1):31-39. doi:10.2174/1872214810666160615102809
45. Rebelos E, Rinne JO, Nuutila P, Ekblad LL. Brain glucose metabolism in health, obesity, and cognitive decline—does insulin have anything to do with it? *A Narrative Review J Clin Med*. 2021;10(7):1532. doi:10.3390/jcm10071532
46. Murai T, Matsuda S. Metabolic reprogramming toward aerobic glycolysis and the gut microbiota involved in the brain amyloid pathology. *Biology (Basel)*. 2023;12(8):1081. doi:10.3390/biology12081081
47. Dienel GA. Brain glucose metabolism: integration of energetics with function. *Physiol Rev*. 2019;99(1):949-1045. doi:10.1152/physrev.00062.2017
48. Fox PT, Raichle ME, Mintun MA, Dence C. Nonoxidative glucose consumption during focal physiologic neural activity. *Science*. 1988;241(4864):462-464. doi:10.1126/science.3260686
49. Prichard J, Rothman D, Novotny E, et al. Lactate rise detected by ^{1}H NMR in human visual cortex during physiologic stimulation. *Proc Natl Acad Sci U S a*. 1991;88(13):5829-5831. doi:10.1073/pnas.88.13.5829

50. Vaishnavi SN, Vlassenko AG, Rundle MM, Snyder AZ, Mintun MA, Raichle ME. Regional aerobic glycolysis in the human brain. *Proc Natl Acad Sci U S a*. 2010;107(41):17757-17762. doi:10.1073/pnas.1010459107
51. Goyal, MS, Vlassenko, AG, Blazey, TM, et al. Loss of brain aerobic glycolysis in normal human aging. *Cell Metab* 2017;26(2):353-360.e3, doi:10.1016/j.cmet.2017.07.010.
52. Medina MA. Metabolic reprogramming is a hallmark of metabolism itself. *Bioessays*. 2020;42(10):e2000058. doi:10.1002/bies.202000058
53. Johansen DH, Albannay MM, Petersen JR, Zhurbenko V, Ardenkjaer-Larsen JH. PIN diode driver for NMR and MRI. *J Magn Reson*. 2019;300:114-119. doi:10.1016/j.jmr.2019.01.017
54. Ha S, Hamamura MJ, Nalcioglu O, Muftuler LT. A PIN diode controlled dual-tuned MRI RF coil and phased array for multi nuclear imaging. *Phys Med Biol*. 2010;55(9):2589-2600. doi:10.1088/0031-9155/55/9/011
55. Choi CH, Hong SM, Ha Y, Shah NJ. Design and construction of a novel $^{1}H/^{19}F$ double-tuned coil system using PIN-diode switches at 9.4T. *J Magn Reson*. 2017;279:11-15. doi:10.1016/j.jmr.2017.04.005
56. Han S-D, Heo P, Kim H-J, et al. Double-layered dual-tuned RF coil using frequency-selectable PIN-diode control at 7-T MRI. *Concepts in Magnetic Resonance Part B: Magnetic Resonance Engineering*. 2017;47B(4):e21363. doi:10.1002/cmr.b.21363
57. Choi CH, Hong SM, Felder J, Shah NJ. The state-of-the-art and emerging design approaches of double-tuned RF coils for X-nuclei, brain MR imaging and spectroscopy: a review. *Magn Reson Med*. 2020;72:103-116. doi:10.1016/j.mri.2020.07.003
58. Zhu X-H, Chen W. *In vivo* ^{17}O MRS imaging—quantitative assessment of regional oxygen consumption and perfusion rates in living brain. *Anal Biochem*. 2017;529:171-178. doi:10.1016/j.ab.2016.08.026
59. Guo R, Zhao Y, Li Y, et al. Simultaneous QSM and metabolic imaging of the brain using SPICE: further improvements in data acquisition and processing. *Magn Reson Med*. 2021;85(2):970-977. doi:10.1002/mrm.28459
60. Li Y, Zhao Y, Guo R, et al. Machine learning-enabled high-resolution dynamic deuterium MR spectroscopic imaging. *IEEE Trans Med Imaging*. 2021;40(12):3879-3890. doi:10.1109/TMI.2021.3101149
61. Song H, Fisher J, Ozen AC, et al. Quantification of regional $CMRO_2$ in human brain using dynamic ^{17}O-MRI at 3T. *Z Med Phys*. 2023. doi:10.1016/j.zemedi.2023.07.004
62. Adamson PM, Datta K, Watkins R, Recht LD, Hurd RE, Spielman DM. Deuterium metabolic imaging for 3D mapping of glucose metabolism in humans with central nervous system lesions at 3T. *Magn Reson Med*. 2024;91(1):39-50. doi:10.1002/mrm.29830

Abbreviations: CMR_{Glc}, cerebral metabolic rate of glucose consumption; CMR_{Lac}, cerebral metabolic rate of lactate formation; $CMRO_2$, cerebral metabolic rate of oxygen consumption; V_{TCA}, cerebral metabolic rate of the tricarboxylic acid cycle.

SUPPORTING INFORMATION

Additional supporting information can be found online in the Supporting Information section at the end of this article.

How to cite this article: Zhang G, Jenkins P, Zhu W, Chen W, Zhu X-H. Simultaneous assessment of cerebral glucose and oxygen metabolism and perfusion in rats using interleaved deuterium (^{2}H) and oxygen-17 (^{17}O) MRS. *NMR in Biomedicine*. 2025;38(1):e5284. doi:10.1002/nbm.5284